An improved model for air–sea exchange of elemental mercury in MITgcm-ECCOv4-Hg: the role of surfactants and waves

Ling Li[1,2], Peipei Wu[3], Peng Zhang[1], Shaojian Huang[1], Yanxu Zhang[4,*]

[1]School of Atmospheric Sciences, Nanjing University, Nanjing, Jiangsu 210023, China

[2]Frontiers Science Center for Critical Earth Material Cycling, Nanjing University, Nanjing, Jiangsu 210023, China

[3]Scripps Institution of Oceanography, University of California San Diego, La Jolla, CA, USA

[4]Department of earth and environmental sciences, Tulane University, New Orleans, LA, 70118, USA

**Correspondence to*: yzhang127@tulane.edu

Abstract. The air–sea exchange of elemental mercury (Hg^0) plays an important role in the global Hg cycle. Existing air–sea exchange models for Hg^0 have not considered the impact of sea surfactants and wave breaking on the exchange velocity, leading to insufficient constraints on the flux of Hg^0. In this study, we have improved the air–sea exchange model of Hg^0 in the three-dimensional ocean transport model MITgcm by incorporating sea surfactants and wave breaking processes through parameterization utilizing the total organic carbon concentration and significant wave height data. The inclusion of these factors results in an increase of 62-225% ~~over twofold~~ in the global transfer velocity of Hg^0 relative to the baseline model. Air–sea exchange flux is increased in mid- to high-latitude regions with high wind and wave breaking efficiency, while it is reduced by surfactant and concentration change at low latitudes with low wind speeds and nearshore areas with low wave heights. Compared with previous parameterizations, the updated model demonstrates a stronger dependence of Hg^0 air–sea exchange velocity on wind speed. Our results also provide a theoretical explanation for the large variances in estimated transfer velocity between different schemes.

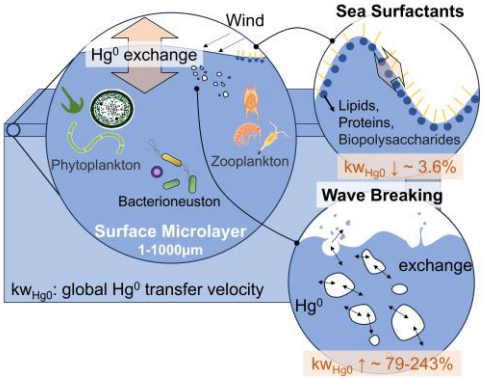

1 Introduction

Air–sea exchange of elemental mercury (Hg^0) contributes up to one-third of the total atmospheric mercury (Hg) emissions. This process is crucial for the global Hg cycle, as it prolongs the residence time of Hg in the biosphere (Amos et al., 2015) and reduces the reservoir of divalent mercury (Hg^{II}) in the surface ocean (Lavoie et al., 2013). The air–sea exchange flux of Hg^0 is generally controlled by both kinetic (gas transfer velocity, k_{Hg^0} ~~k_{Hg}~~) and thermodynamic (partial pressure related concentration gradients) forcing (Wanninkhof, 1992; Wanninkhof et al., 2009; Kuss et al., 2011). However, the lack of direct measurements of Hg^0 transfer velocity results in substantial uncertainty in estimating large-scale air–sea Hg^0 exchange (Zhang et al., 2019). Considering that wind is the primary force driving turbulence in the upper ocean, the transfer velocity is typically parameterized with wind speed through linear (Jähne et al., 1979; Liss and Merlivat, 1986), quadratic (Wanninkhof et al., 1992; Nightingale et al., 2000), or cubic relationships (McGillis et al., 2001; Edson et al., 2011). The estimated magnitude of global air–sea exchange of Hg ranges from to 2840 Mg a^{-1} to 3950 Mg a^{-1} (Zhang et al., 2019; Liss and Merlivat, 1986; Wanninkhof et al., 1992; McGillis et al., 2001; Zhang et al., 2023). Osterwalder et al. (2021) further demonstrated that different transfer velocity parameterizations can lead to more than a fourfold variation in sea-air exchange flux estimates along the coastal Baltic Sea (0.3±0.6 ng m^{-2} h^{-1} to 2.6±0.6 ng m^{-2} h^{-1}). However,~~In addition,~~ the gas transfer velocity is influenced by other environmental factors such as surfactants and waves (Wurl et al., 2017). Therefore, relying solely on wind speed may not be sufficient to quantify k_{Hg^0} ~~k_{Hg}~~.

Field Code Changed

Field Code Changed

Surfactants are ubiquitous in the sea surface microlayer (SML) and have associations with marine biological ~~production~~ activity (Lin et al., 2002; Wurl et al, 2011). ~~Surfactants~~ They are generally believed to affect air–sea exchange in two ways: first, surfactants act as a physicochemical barrier that suppresses Hg^0 air–sea exchange~~.~~ , ~~Second~~second, surfactants alter sea surface hydrodynamics, thus affecting turbulent energy transfer (McKenna and McGillis, 2004; Engel et al., 2017), microscale fragmentation, and surface renewal processes. Both experimental and modelling studies reveal that surfactants have a significant inhibitory effect on the transfer velocity of various gases. Notably, a field experiment demonstrated that the injection of artificial surfactant resulted in a suppression of transfer velocity (kw) by up to 55% (Salter et al., 2011). Mesarchaki et al. (2015) observed that surfactants reduced the transfer velocity of N_2O by up to a factor of three in a large-scale wind-wave tank. Modelling research has shown that surfactants could reduce global net CO_2 exchange by 15–50% (Asher, 1997; Tsai and Liu, 2003; Wurl et al., 2016). Studies conducted by Kock et al. (2012) in the equatorial North Atlantic demonstrated an overestimation of N_2O using conventional kw methods, while the scheme considering the effect of surfactants (Tsai and Liu, 2003) aligned well with the observations. Nevertheless, the impact of surfactants on the Hg^0 air–sea exchange remains unknown.

Breaking waves produce bubbles that significantly facilitate the gas fluxes by increasing the air–water interface and intensifying turbulence as the bubbles rise (Asher et al. 1996; Wanninkhof et al. 2009). This is particularly pronounced for insoluble gases (Woolf and Thorpe, 1991; Kihm and

Kortzinger, 2010; Vagle et al., 2010). Woolf (1997) estimated that bubbles contribute about 30-50% to the global CO_2 transfer velocity, assuming a proportional relationship between bubble-mediated transfer velocity and whitecap fraction. Historically, several models have been proposed to determine CO_2 exchange at the sea surface. Zhang et al. (2006) found that the enhancement of gas transfer velocity for O_2 and N_2 due to bubbles can be as high as 20%. According to Reichel and Deike (2020), approximately 40% of the net CO_2 flux between the air and the ocean is attributed to bubbles. The significance of bubble effects depends on the solubility of gases in seawater. It is anticipated that bubble effects will be more pronounced for Hg^0, given its lower solubility. ~~The importance of bubble effects depends on the solubility of gases in seawater, and it is expected to be more significant for Hg^0 with lower solubility.~~

In this study, we have improved the MITgcm ocean model to gain a better understand of the mechanisms that govern the air–sea exchange of Hg^0 at the atmosphere–ocean interface by including the effects of surfactants and wave breaking process. Sensitivity experiments are also conducted to analyze the effects of individual factors on the Hg^0 transfer velocity. Additionally, we have examined the dependence of Hg^0 transfer velocity on wind speed.

2 Methodology

2.1 MITgcm model

The MITgcm (http://mitgcm.org/) is employed to simulate the air–sea exchange of Hg^0. We use a configuration that has been fit to observations in a least-squares approach (ECCO v4; Forget et al., 2015). This three-dimensional configuration features a horizontal resolution of 1°×1° and comprises 50 vertical layers. Near the equator (0.5° latitude × 1° longitude) and the Arctic (approximately 40 km × 40 km), a higher horizontal resolution is adopted to better simulate ocean currents. It calculates ocean physical processes including vertical advection, diapycnal diffusion, and convective mixing based on ocean state estimates from ECCO v4. The meteorological field of atmospheric variables (temperature, wind stress, precipitation, humidity, and radiation) serves as the boundary layer of ocean are from the 6-hour ERA-Interim reanalysis, spanning 1992 to 2017.

The model has the capacity to simulate the marine Hg cycles, which include the redox conversion between Hg^0 and Hg^{II}, the methylation and demethylation of monomethylmercury (CH_3Hg) and dimethylmercury [$(CH_3)_2Hg$], the air–sea exchange of Hg^0 and $(CH_3)_2Hg$, the partitioning between dissolved and particulate mercury, the sinking of particulate-bound Hg, and the bioaccumulation of CH_3Hg in marine food webs (Zhang et al., 2014; 2020). Biogeochemical and ecological variables, such as ~~primary productivity (PP),~~ particulate organic carbon (POC) and dissolved organic carbon (DOC) in the ocean, are obtained from the Darwin marine ecosystem model (the DARWIN project: http://darwinproject.mit.edu/; Dutkiewicz et al., 2012).

The air–sea exchange of Hg^0 (eq.1) is calculated from the exchange velocity (kw_{Hg^0}) and the concentration gradient of Hg^0 across the air–sea interface corrected normalized by dimensionless Henry's

Formatted: Superscript

Formatted: Default Paragraph Font, Font: (Default) +Body (等线), 五号
Formatted: Font: 10 pt, Not Italic
Formatted: Font: 10 pt, Not Italic, Superscript
Formatted: Font: 10 pt, Not Bold, Not Italic
Formatted: Font: 10 pt, Not Italic
Formatted: Font: 10 pt, Not Italic
Field Code Changed
Formatted: Font: 10 pt, Not Italic, Superscript
Formatted: Font: 10 pt, Not Italic
Formatted: Font: 10 pt
Formatted: Font: 10 pt, Not Italic

law constant ($C_w - C_A/H$) (Andersson et al., 2008). Where Cw and C_A represent the concentration of Hg^0 on the water and air side, respectively, H is the dimensionless Henry's law constant, which quantifies the ability of the dissolved phase to escape into the water. In the baseline parameterization, the exchange velocity of Hg^0 on the ocean side (eq. 2) is estimated following the quadratic relationship with wind speed proposed by Nightingale et al. (2000) for CO_2 (eq. 3) adjusted for the Schmidt number of Hg^0 (Sc_{Hg^0} , eq. 4), and for the proportion of ice-free sea surface areas (1-iceo). For a related parameterization in baseline model, see Zhang et al. (2015).

~~The baseline air–sea exchange of Hg^0 is calculated using the concentration gradient of Hg^0 across the air–sea interface, the Henry's law constant (Andersson et al., 2008), the proportion of ice-free sea surface areas, and the exchange velocity parameterized by wind speed proposed by Nightingale et al. (2000). Additionally, the transfer velocity also depends on the temperature and salinity-corrected Hg^0 diffusion rate in seawater (Wilke and Chang, 1955) and the temperature-corrected Schmidt number for CO_2 (Poissant et al., 2000). Based on the results of Loose et al. (2014), the exchange velocity for partially ice-covered regions is doubled to accommodate the increased shear stress and convectively driven turbulence induced by drifting sea ice. The Hg^0 air–sea flux ($Flux_{Hg^0}$) is calculated as follows:~~

$$Flux_{Hg^0} = k_{Hg^0} \times (C_w - C_A/H) \quad (1)$$

~~Where C_w and C_A represent the concentration of Hg^0 on the water and air side, respectively, H is the Henry's law constant, which quantifies the ability of the dissolved phase to escape into the water, and k_{Hg^0} is the transfer velocity of Hg^0 on the ocean side calculated as follows:~~

$$k_{Hg^0} = (1 - iceo) \times k_{600} / \sqrt{Sc_{Hg^0}/Sc_{CO_2}} \quad (2)$$

~~where~~

$$k_{600} = 0.222 \cdot u_{10}^2 + 0.333 \cdot u_{10} \quad (3)$$

~~Where $iceo$ is the sea ice coverage, Sc_{Hg^0} and Sc_{CO_2} are the Schmidt numbers for Hg^0 and CO_2, respectively. k_{600} is the piston velocity of CO_2 given by Nightingale et al. (2000).~~ ~~The~~We modified expression for the air–sea exchange velocity (eq.7), ~~which~~ takes into account the effects of surfactants and wave breaking, which will be described in more detail in the following two sections. ~~is given by the following equation:~~

$$kw_{Hg^0} = (1 - iceo) \times [k_{int} + k_{bub}] \times (1 - Skw[\%]/100) \quad (14)$$

We conduct a total of eight simulations (Table 2), including one baseline simulation, four simulations that comprehensively consider the effects of wave breaking and surfactants: Case1 (~~P18~~SUR1 + ~~DM18~~WB1), Case2 (~~P18~~SUR1 + ~~W97~~WB2), Case3 (~~P18~~SUR1 + ~~AW98~~WB3), and Case4 (~~P18~~SUR1 + ~~A02~~WB4), and three sensitive experiments that solely consider the effects of

Formatted: Font: 10 pt, Not Bold, Not Italic
Formatted: Font: 10 pt, Not Italic
Formatted: Subscript
Field Code Changed
Formatted: Superscript
Formatted: Font: 10 pt, Not Italic
Formatted: Font: Not Italic
Formatted: Font: Not Italic, Superscript
Formatted: Font: Not Italic
Formatted: Font: Not Bold, Not Italic
Formatted: Font: Not Bold, Not Italic
Formatted: Font: Not Italic
Formatted: Font: Not Bold, Not Italic
Formatted: Font: Not Bold, Not Italic, Subscript
Formatted: Font: Not Italic
Formatted: Font: Not Bold, Not Italic
Formatted: Font: Not Italic
Formatted: Font: Not Italic, Superscript
Formatted: Font: Not Italic
Formatted: Font: (Default) Times New Roman
Formatted: Font: Not Italic
Formatted: Font: Not Italic
Field Code Changed

Formatted: Justified, Indent: Left: 0.37 cm, Right: 0.37 cm, First line: 0 ch

surfactants (Case5A, P18SUR1) and wave breaking (Case6B, DM18WB1 and Case7C, AW98WB3).

The model is run from 1992 to 2011, allowing the response of Hg species to ocean physical and biogeochemical changes to reach a steady state. The initial conditions are extracted from the previous model output conducted by Zhang et al. (2020).

2.2 Parameterization of surfactants

Formatted: Heading2(GMD), Space After: 0 pt, Line spacing: single, Snap to grid

Surfactants are mainly originated from ocean biological activities (Lin et al., 2002), with elevated concentrations anticipated in regions characterized by increased primary productivity (PP) (Wurl et al., 2011). The concentration of surfactants at the sea surface isSea surface surfactant concentrations are related to PP, which is commonly represented by estimated from chlorophyll a (Chl a) (Tsai and Liu, 2003) for operational reasons (i.e. remote sensing)(Tsai and Liu, 2003). Nevertheless, recent studies have shown that Chl a cannot fully predict the occurrence of surface surfactants when used as a substitute for PP (Wurl et al., 2011; Sabbaghzadeh et al., 2017). Some strains of heterotrophic bacteria are known to produce surfactants (Satpute et al., 2010) and have been linked to a surfactant-covered ocean surface (Kurata et al., 2016). Additionally, the occurrence of surfactants is also subject to influence from meteorological conditions, including solar radiation (Gasparovic et al., 1998) and precipitation (Wurl and Obbard, 2005). Surface tension (Schmidt and Schneide, 2011), organic carbon concentration (Calleja et al., 2009; Barthelmeß et al., 2021), and sea surface temperature (Pereira, 2018) are also used to predict the occurrence of surface surfactants. However, most studies have not provided a clear quantitative relationship.

We model the influence of surfactants concentration ([SA]) on transfer velocity (eq. 8) based on the empirical equation derived by Pereira et al. (2018) from a shipboard gas exchange tank experiment in the Atlantic Ocean. And we adopt a relationship following Barthelmeß (2021) who found a linear relationship between concentration of total organic carbon ([TOC]) and [SA] in the Atlantic Ocean (eq. 9). We adopt a relationship following Barthelmeß (2021) who found a linear relationship between total organic carbon (TOC) and surface surfactant concentration in the Atlantic Ocean:

$$[SA] = 0.007[TOC] - 0.38 \quad (4)$$

where $[SA]$ represents the concentration of surface surfactants (mg TX-100 equiv. L^{-1}) and $[TOC]$ represents the concentration of TOC (μM) at the sea surface.

We model the influence of surfactants on piston velocity based on the empirical equation derived by Pereira et al. (2018) from a shipboard gas exchange tank experiment in the Atlantic Ocean:

$$Skw[\%] = 32.44[SA] + 2.51 \quad (5)$$

where $Skw[\%]$ is the suppression of air–sea exchange velocity by surface surfactants. Therefore, a parameterization (hereafter referred to as P18SUR1) was derived using the concentration of TOC

on at the sea surface as an indicator of the suppression of air–sea exchange velocity by surface surfactants ($Skw[\%] = 0.227[TOC] - 9.817$).

$$Skw[\%] = 0.227[TOC] - 9.817 \quad (6)$$

2.2 3 Parameterization of wave breaking

To take into account the effect of wave breaking on the air–sea exchange velocity, we separate the contributions of wave breaking (k_{bub}) and non-breaking (k_{int}) following the approach of Woolf (2005). The model agrees with measurements of CO_2 transfer at 20°C, but does not account for the dependence of k_{bub} on solubility. Therefore, this model is exclusively applicable to CO_2 and necessitates modifications for Hg^0 compatibility (Jeffery et al., 2010). Here we take the influence of solubility into consideration. For the non-breaking part, we utilize the squared wind speed parameterization (Nightingale et al., 2000) previously adopted in the model (eq. 2).

$$k_{int} = k_{600} / \sqrt{Sc_{Hg^0} / Sc_{CO_2}} \quad (7)$$

Regarding the wave breaking component, we attempt to use four different parameterization schemes, all considering the significant wave height (Hs), friction velocity (u*) and Ostwalt solubility (α, unitless). Hs has been proved to be we attempt to use four different parameterization schemes. We include significant wave height (H_s), which has been proved to be a more direct physical variable to estimate air–sea exchange (Li et al., 2021). The Hs dataHere we use are climatological monthly mean for the 2000–2020 obtained from ERA5 reanalysis data (Hersbach et al., 2020). u* is represented by a piecewise linear function of the wind speed (eq. 10), as given by Edson (2013). And α is expressed according to Battino (1984) and Andersson et al. (2008) (eq.11).

The first parameterization utilizes a sea-state dependent gas transfer velocity parameterization developed by Deike and Melville (2018), hereafter referred to as WB1 (eq. 12). A_B is dimensional fitting coefficient. The WB1 parameterization is based on direct numerical simulations of bubble dynamics beneath breaking waves (Deike et al., 2016), as well as observations and modeling of wave and wave-breaking statistics (Deike et al., 2017). It has been validated by field measurements of gas transfer velocity (Bell et al., 2017; Brumer et al., 2017).

The first last three parameterizations (Woolf, 1997; Asher and Wanninkhof, 1998; Asher et al., 2002) calculate the bubble-mediated transfer velocity (eq. 13-15, hereafter referred to as WB2-4) as a function of total whitecap coverage (Wc). Total whitecap coverage encompasses :Woolf (1997), hereafter referred to as W97:

$$k_{bub} = \frac{2450 W_C}{\alpha \left(1 + \left(14 \alpha Sc_{Hg^0}{}^{-0.5}\right)^{-1/1.2}\right)^{1.2}} \quad (10)$$

Formatted: Font: 10 pt

Field Code Changed

Formatted: Justified, Indent: First line: 0 ch

Formatted: Justified, Indent: First line: 0 ch

Formatted: Justified, Indent: Left: 0.37 cm, Right: 0.37 cm, First line: 0 ch

Asher and Wanninkhof (1998), hereafter referred to as AW98:

$$k_{bub} = W_C\left(\frac{-37}{\alpha} + 6120\alpha^{-0.37}Sc_{Hg^0}^{-0.18}\right) \quad (8)$$

Asher et al. (2002), hereafter referred to as A02:

$$k_{bub} = W_C\left(\frac{-37}{\alpha} + 10440\alpha^{-0.41}Sc_{Hg^0}^{-0.24}\right) \quad (9)$$

Woolf (1997), hereafter referred to as W97:

$$k_{bub} = \frac{2450W_C}{\alpha\left(1+\left(14\alpha Sc_{Hg^0}^{-0.5}\right)^{-1/1.2}\right)^{1.2}} \quad (10)$$

where α represents Ostwalt solubility (unitless), which is expressed according to Battino (1984) and Andersson et al. (2008). W_C represents the total whitecap coverage (unitless), encompassing both the breaking crest generated by recent wave breaking (stage A whitecaps, W_A) and the sea surface foam in the process of decay (stage B whitecaps, W_B). W_A might be a better parameter for bubble-mediate transfer velocity, owing to its more direct relationship with energy dissipation. Nevertheless, it exhibits weak correlation with the Reynolds number and presents challenges in measurement. Therefore, we have opted to employ the concept of total whitecap coverage for our calculations. It should also be pointed that, in the case of AW98WB3 and A02WB4, we have focused exclusively on transfer via direct bubble exchange, which provides a better simulateion of the transfer velocity (Blomquist et al., 2017). W_C (eq. 16) is a function of the wind sea Reynolds number (eq.17) (RH, proposed by Woolf et al. (, 2005), which is estimated with friction velocity, significant wave height and air kinematic viscosity.):

$$Wc = 4.02\times10^{-7}\times RH^{0.96} \quad (11)$$

where

$$RH = \frac{u^* H_s}{\upsilon_\alpha} \quad (12)$$

where u* is the friction velocity, and υ_α is the air kinematic viscosity, with a value of $1.48\times10^{-5}\ m^2/s$ at a temperature of 20℃.

The fourth parameterization utilizes a sea-state dependent gas transfer velocity parameterization developed by Deike and Melville (2018), hereafter referred to as DM18. The DM18 parameterization is based on direct numerical simulations of bubble dynamics beneath breaking waves (Deike et al., 2016), as well as observations and modeling of wave and wave-breaking statistics (Deike et al., 2017). It has been validated by field measurements of gas transfer velocity (Bell et al., 2017; Brumer et al., 2017):

Formatted: Justified, Indent: Left: 0.37 cm, Right: 0.37 cm, First line: 0 ch

Formatted: Justified, Indent: Left: 0.37 cm, Right: 0.37 cm, First line: 0 ch

Formatted: Justified, Indent: Left: 0.37 cm, Right: 0.37 cm, First line: 0 ch

Formatted: Justified, Indent: Left: 0.37 cm, Right: 0.37 cm, First line: 0 ch

Formatted: Justified, Indent: Left: 0.37 cm, Right: 0.37 cm, First line: 0 ch

~~$$k_{bub} = \frac{A_B}{\alpha}[u_*^{5/3}\sqrt{gH_s}^{4/3}]$$ (13)~~

~~where A_B is dimensionless fitting coefficient (A_B=1±0.2×10^{-5} s^2 m^{-2}). The friction velocity (u*) is represented by a piecewise linear function of the wind speed, as given by Edson (2013).~~

~~The expression for the air–sea exchange velocity, which takes into account the effects of surfactants and wave breaking, is given by the following equation:~~

$$K_{Hg^0} = (1-iceo)\times[k_{int}+k_{bub}]\times(1-Suppression\ of\ kw[\%]/100)$$ ~~(14)~~

Detailed parameterization and introduction of variables are listed in Table 1.

Table 1. Model equation of air-sea exchange and parameterizations for wave breaking and surfactant

Variables	Units	Description	Value or equation	equation number
$Flux_{Hg^0}$	ug m^{-2} a^{-1}	Hg^0 air–sea flux	$Flux_{Hg^0} = kw_{Hg^0}\times(C_w - C_A/H)$	(1)
$k_{int\_Hg^0}$	cm h^{-1}	Initiate transfer velocity of Hg^0	$k_{int\_Hg^0} = (1-iceo)\times k_{600}/\sqrt{Sc_{Hg^0}/Sc_{CO_2}}$	(2)
k_{600}	cm h^{-1}	CO_2 transfer velocity normalized to Sc=600	$k_{600} = 0.222\cdot u_{10}^{\ 2} + 0.333\cdot u_{10}$	(3)
Sc_{Hg^0}	Unitless	Schmidt number of Hg	$Sc_{Hg^0} = \upsilon_w/D_{Hg^0}$	(4)
υ_w	cm^2 s^{-1}	Kinematic viscosity of water	$\upsilon_w = 0.017\exp(-0.025T)$	(5)
D_{Hg^0}	cm^2 s^{-1}	Hg diffusivity in water	$D_{Hg^0} = 6\times10^{-7}T + 1\times10^{-5}$	(6)
kw_{Hg^0}	cm h^{-1}	Modified transfer velocity of Hg^0	$kw_{Hg^0} = (1-iceo)\times[k_{int}+k_{bub}]\times(1-Skw[\%]/100)$	(7)
$Skw[\%]$	Unitless	Suppression of air–sea exchange velocity by surface surfactants	$Skw[\%] = 32.44[SA] + 2.51$	(8)
[SA]	mg TX-100 equiv. L^{-1}	Concentration of surface surfactants	$[SA] = 0.007[TOC] - 0.38$	(9)
TOC	mol l^{-1}	Sea surface total organic carbon concentration	TOC=DOC+POC	
DOC	mol l^{-1}	Sea surface dissolved organic carbon concentration	Darwin model	
POC	mol l^{-1}	Sea surface particle organic carbon concentration	Darwin model	
u*	m s^{-1}	Friction velocity [f]	$u_* = \begin{cases} 0.03\times u_{10}, & u_{10} < 4\ m/s \\ 0.035\times u_{10}, & 4\ m/s < u_{10} < 8.5\ m/s \\ 0.062\times u_{10} - 0.28, & u_{10} > 8.5\ m/s \end{cases}$	(10)
α	Unitless	Ostwalt solubility [e]	$\alpha = exp((-2404.3/t) + 6.92)$	(11)

Formatted Table
Formatted: Font: 小五
Formatted: Font: Times New Roman, 小五
Formatted: Font: 小五
Formatted: Superscript
Formatted: Font: 小五
Formatted: Font: (Default) Times New Roman, (Asian) 宋体, 小五
Formatted: Font: 小五
Formatted: Font: (Default) Times New Roman, 小五
Formatted: Font: (Default) Times New Roman, 小五
Formatted: Font: 小五
Formatted: Font: 小五, Superscript
Formatted: Font: (Asian) 宋体, 小五
Formatted: Font: (Default) Times New Roman, (Asian) 宋体, 小五
Formatted: Subscript
Formatted: Font: 小五
Formatted: Font: 小五
Formatted: Font: (Asian) 宋体
Formatted: Font: 小五
Formatted: Font: 小五
Formatted: Font: 小五
Formatted: Font: 小五
Formatted: Font: (Asian) 宋体
Formatted: Font: 小五
Formatted: Font: 小五
Formatted: Font: 小五
Formatted: Font: (Default) Times New Roman

			$WB1: k_{bub} = \frac{A_B}{\alpha}[u_*^{5/3}\sqrt{gH_s}^{4/3}]$	(12)~~(11)~~
k_{bub}	m s^{-1}	Bubble mediated gas transport rate[a,b,c,d]	$WB2: k_{bub} = \frac{2450W_C}{\alpha\left(1+\left(14\alpha Sc_{Hg^0}^{-0.5}\right)^{-1/1.2}\right)^{1.2}} / 360000$	(13)~~(12)~~
			$WB3: k_{bub} = W_C\left(\frac{-37}{\alpha} + 6120\alpha^{-0.37}Sc_{Hg^0}^{-0.18}\right) / 360000$	(14)~~(13)~~
			$WB4: k_{bub} = W_C\left(\frac{-37}{\alpha} + 10440\alpha^{-0.41}Sc_{Hg^0}^{-0.24}\right) / 360000$	(15~~4~~)
A_B	s^2 m^{-2}	Dimensional fitting coefficient [a]	$1\pm0.2\times10^{-5}$	
Wc	Unitless	Total whitecap coverage factor [g]	$Wc = 4.02\times10^{-7}\times RH^{0.96}$	(16)
RH	Unitless	wind sea Reynolds number [g]	$RH = \frac{u^*Hs}{\upsilon_\alpha}$	(17)
υ_α	m^2 s^{-1}	Kinematic viscosity at 20℃	1.48×10^{-5}	
g	m s^{-2}	Acceleration of gravity	9.807	
Hs	m	Significant wave height	ERA5 monthly data	

[a] Poissant et al., 2000.
[b] Deike and Melville, 2018.
[c] Woolf et al., 1997.
[d] Asher and Wanninkhof, 1998.
[e] Asher et al., 2002.
[f] Battino, 1984; Andersson et al., 2008.
[g] Edson et al., 2013.
[h] Woolf et al., 2005

~~**Table 1.** Model parameterizations for wave breaking and surfactant~~

~~Variables~~	~~Units~~	~~Description~~	~~Value or equation~~
~~Suppression of kw[%]~~	~~Unitless~~	~~Suppression of air–sea exchange velocity by surfactants~~	~~*Suppression of kw*[%] = 0.227[*TOC*] – 9.817~~
~~TOC~~	~~mol l^{-1}~~	~~Sea surface total organic carbon concentration~~	~~TOC=DOC+POC~~
~~DOC~~	~~mol l^{-1}~~	~~Sea surface dissolved organic carbon concentration~~	~~Darwin model~~
~~POC~~	~~mol l^{-1}~~	~~Sea surface particle organic carbon concentration~~	~~Darwin model~~

Formatted Table
Formatted: Font: (Default) Times New Roman
Formatted: Font color: Auto, (Asian) Chinese (Simplified, Mainland China), (Other) English (United States)
Formatted: Font: (Default) Times New Roman, (Asian) 宋体
Formatted: Font: (Default) Times New Roman, (Asian) 宋体, 小五
Formatted: Not Superscript/ Subscript

			$k_{bub} = \frac{A_B}{\alpha}[u_*^{3/3}\sqrt{gH_s}^{4/3}]$ [a]
			$k_{bub} = \frac{2450W_C}{\alpha\left(1+\left(14\alpha Sc_{Hg^0}{}^{-0.5}\right)^{1/1.2}\right)^{1.2}} / 360000$ [b]
k_{bub}	m s^{-1}	Bubble mediated gas transport rate	$k_{bub} = W_C\left(\frac{-37}{\alpha} + 10440\alpha^{-0.41}Sc_{Hg^0}{}^{-0.24}\right) / 360000$ [c]
			$k_{bub} = W_C\left(\frac{-37}{\alpha} + 6120\alpha^{-0.37}Sc_{Hg^0}{}^{-0.18}\right) / 360000$ [d]
A_B	s^2 m^{-2}	Dimensional fitting coefficient [a]	$1\pm0.2\times10^{-5}$
α	Unit less	Ostwalt solubility [e]	$\alpha = exp((-2404.3/t)+6.92)$
u^*	m s^{-1}	Friction velocity [f]	$u_* = \begin{cases} 0.03\times u_{10}, & u_{10} < 4\ m/s \\ 0.035\times u_{10}, & 4\ m/s < u_{10} < 8.5\ m/s \\ 0.062\times u_{10} - 0.28, & u_{10} > 8.5\ m/s \end{cases}$
Wc	Unit less	Total whitecap coverage factor [g]	$Wc = 4.02\times10^{-7}\times RH^{0.96}$; $RH = \frac{u^* H_s}{\upsilon_\alpha}$
RH	Unit less	wind sea Reynolds number [g]	
υ_α	m^2 s^{-1}	Kinematic viscosity	1.48×10^{-5}
g	m s^{-2}	Acceleration of gravity	9.807
H_s	m	Significant wave height	ERA5 monthly data

[a] Deike and Melville, 2018.
[b] Woolf et al., 1997.
[c] Asher and Wanninkhof, 1998.
[d] Asher et al., 2002.
[e] Battino, 1984; Andersson et al., 2008.
[f] Edson et al., 2013.
[g] Woolf et al., 2005

We conduct a total of eight simulations, including one baseline simulation, four simulations that comprehensively consider the effects of wave breaking and surfactants: Case1 (P18 + DM18), Case2 (P18 + W97), Case3 (P18 + AW98), and Case4 (P18 + A02), and three sensitive experiments that solely consider the effects of surfactants (Case5, P18) and wave breaking (Case6, DM18 and Case7, AW98).

Table 2. Experimental setting

Parameterizations	Surfactants	Wave Breaking			
	P18[a]SUR1[a]	DM18[a]WB1[b]	WBW927[c]	WB3AW98[d]	WB4A02[e]
Baseline					
Case1	√	√			

Case2	√		√		
Case3	√			√	
Case4	√				√
~~Case5~~CaseA	√				
~~Case6~~CaseB		√			
~~Case7~~CaseC				√	

[a] Pereira et al., 2018
[b] Deike and Melville, 2018.
[c] Woolf et al., 1997.
[d] Asher and Wanninkhof, 1998.
[e] Asher et al., 2002.

2.~~3~~ 4 Observation Datasets

We incorporate observational data from seven cruises that involved high-resolution synchronous measurements of atmospheric and water Hg^0 concentrations in the Atlantic, Pacific and Southern Oceans. These include data obtained by Kuss et al. (2011) during a transect from Punta Arenas, Chile, to Bremerhaven, Germany, across the Atlantic in April–May 2009. Soerensen et al. (2013) reported data from six cruises conducted between 2008 and 2010 in the Gulf of Maine, the New England Shelf, the continental slope region and the Sargasso Sea. They also collected data along a latitudinal transect (~20°N to ~15°S) in the central Pacific during the METZYME cruise in October 2011 (Soerensen et al., 2014). Wang et al. (2017) obtained data during a cruise along the Antarctic coast from December 13, 2014 to February 1, 2015. Kalinchuk et al. (2020) reported data from a public cruise in the eastern Arctic Ocean from September 7 to October 30, 2018. Mastromonaco et al. (2017) measured continuously in the remote seas of western Antarctica, including Weddell Sea during winter and spring (2013) and Bellingshausen, Amundsen and Ross seas during summer (2010/2011). All of these studies used similar measurement methods, including Tekran trace mercury analyzers for atmospheric Hg^0 measurements and automated continuous equilibrium systems for seawater Hg^0 measurements. The Hg^0 flux was calculated based on a thin film gas exchange model (equation 1; Liss and Merlivat, 1986; Wanninkhof, 1992). The transfer velocity was calculated using the Nightingale et al. (2000) or Wanninkhof (1992) parametrization for instantaneous wind speeds, both characterized by a quadratic relationship with wind speed. The reported data frequencies varied from 1 to 10 hours. Observational data on various forms of Hg concentrations at the sea surface are summarized in Zhang et al. (2020).

3 RESULTS AND DISCUSSION

3.1 Suppression of k_{Hg^0} ~~kw~~ by surfactants

Field Code Changed

Figure 1 presents the air–sea exchange velocity calculated by the baseline model and the suppression rate of kw_{Hg^0} ~~kw~~ caused by the surface microlayer calculated from the annual average TOC concentrations.

Field Code Changed

The transfer velocity of baseline model is zonally distributed, with higher value (33.5 cm h^{-1}) at mid-to-

high latitudes, attributed to wind-induced turbulence enhancement. In this study, we term it as the transfer velocity of non-breaking waves. Our parameterization of the suppression rate is directly related to the distribution of DOC, which, in turn, is influenced by the biological activity (Hansell et al., 2009). The model simulates a higher suppression rate in tropical and Arctic regions, reaching up to 16.7% (Fig. 1b), but 5–10% in most regions. In tropical regions, organic matter resistant to degradation accumulates due to vertical stratification. In Arctic regions, terrigenous organic matter is transported to the system via high fluvial fluxes (Dittmar and Kattner, 2003). The lowest values are presented in the Southern Ocean, where deep ocean waters are more readily mixed with the surface. This finding is consistent with that of Wurl (2011) who reported a more significant SML coverage between 30°N and 30°S~~–~~. Our estimated suppression effect of surfactants generally aligns with Barthelmeß et al. (2021), who reported a suppression of kw of CO_2 by 11.5% (±SE 1.0) inside and 9.8% (±SE 2.2) outside the filament in the Atlantic Ocean. Similarly, Pereira et al. (2018) found the kw suppressions reduced by 2 to 32% in the Atlantic in the presence of surfactants.

However, it is worth noting that other studies propose a greater impact. According to Pereira et al. (2016), the exchange of CO_2 between the ocean and atmosphere decreased by 15 to 24% along the North East coast of the UK. Furthermore, Yang et al. (2021) reported that the wind speed dependence of CO_2 transfer velocity can vary by 30% in the Southern Ocean. Frew (1997) observed a fivefold reduction in gas transfer velocity near the coast of New England due to increased surfactant abundance and DOC content compared to the open ocean. Our lower estimate of the suppression effect might be reasonable, as their samples were collected at different wind speed, which has significant role in surfactant suppression. The high~~ly~~ variation in molecular composition across diverse environments also leads to a large variation in surface activity (Barthelmeß et al., 2022). ~~-~~Therefore, the ~~linear~~ suppression relationship may change in different environments. Our surfactant parametrization used here was based on data from the Atlantic Ocean which may not be applicable to other regions. Additionally, some research conducted in the laboratory might not fully explain processes in the natural environment (Krall and Jähne, 2014). To better explain the measured differences in Hg^0 emissions between coastal and open ocean areas, we need to improve our understanding of how surfactants and wind speed interact (e.g., marine aerosol emissions, surfactant abundance) to affect Hg^0 air–sea exchange velocity and subsequent net Hg^0 fluxes.

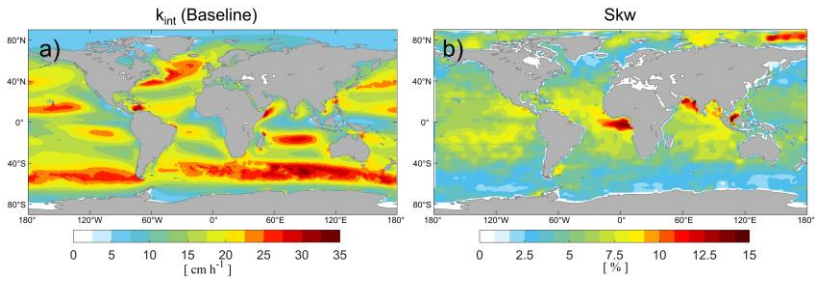

Figure 1. a) The annual mean non-breaking gas transfer velocity in unit of cm h^{-1}. b) The suppression of annual mean Hg^0 gas transfer coefficient (kw_{Hg^0} ~~k_{Hg}~~) by surfactants in unit of %.

Field Code Changed

3.2 Enhancement of kw_{Hg^0} ~~kw~~ by breaking wave

The bubble-mediated transfer velocities, calculated using four different bubble parameterizations, are shown in Fig. 2. The spatial distribution of the velocities is quite similar for all the four scenarios with relatively high values in regions with high wind speeds at mid- and high-latitudes, similar to the exchange velocity of non-braking wave (Fig. 1a). However, the magnitude varies substantially among them. The global mean bubble-mediated transfer velocities are 10.8, 9.9, 26.3 and 33.0 cm h^{-1}, respectively. Bubble-mediated transfer velocities calculated with the ~~DM18~~WB1 parameterization (Fig. 2a) and the ~~W97~~WB2 parameterization (Fig. 2b) are comparable to those of non-breaking waves. Compared to the ~~DM18~~WB1 parameterization, the ~~W97~~WB2 parameterization shows less variation in exchange rates across latitudes, with higher rates in low-latitude regions and lower rates in mid- and high-latitude regions. The reason may be that ~~DM18~~WB1 have higher wind or wave height dependence of kw_{Hg^0} ~~kw~~ than that of ~~W97~~WB2 (Fig. S1). Conversely, the ~~AW98~~WB3 (Fig. 2c) and ~~A02~~WB4 (Fig. 2d) parameterizations significantly enhance the air–sea exchange velocity of Hg^0 (t test on means, $p<0.001$). In the Southern Ocean and the North Atlantic region, bubble-mediated transfer rates can reach 105–120 cm h^{-1}, approximately 2–3 times higher than the transfer rates of non-breaking waves. This can be explained by the employment of total whitecap coverage rather than stage A whitecap (W_A), as W_C is much higher than W_A (Monahan and Woolf, 1989). Case 2–4 might overestimate the bubble mediated transfer velocity. ~~W97~~WB2 was given for clean bubbles in quiescent water. This parameterization ignores bubbles that are mixed to a considerable depth, leading to an underestimation of the transfer velocity of poorly soluble gases (Woolf, 1997). ~~AW98~~WB3 and ~~A02~~WB4 have been corrected for the dual-tracer method in laboratory simulations (Asher and Wanninkhof, 1998), but they were not considered adequately for all cases, which is articulately important as gas transfer is highly sensitive to void fraction (the ratio of air volume to total volume) and bubble plume (Woolf et al., 2007). On the other hand, ~~DM18~~WB1 was developed by combining a mechanistic model for air entrainment and bubble statistics with empirical relationships for wave statistics. It also has a good comparison with measured and model data for different gases (Deike and Melville, 2018). In terms of physical mechanisms, ~~DM18~~WB1 considers the process more comprehensively. Therefore, we suggest that ~~DM18~~WB1 might provide a better parameterization of wave breaking.

Our results demonstrate a higher contribution of wave breaking and bubbles to Hg^0 air–sea exchange flux than CO_2. The bubble mediated transfer velocity in most regions is comparable with nonbreaking transfer velocity, and it can reach up to 2–3 times as high as nonbreaking transfer velocity at high wind speed region. But bubble transfer velocity of CO_2 accounts for a comparatively ~~relatively~~ small proportion in transfer velocity according to previous studies (Woolf et al., 1997; Reichel and Deike, 2020). Woolf (1997) estimated that bubbles contribute about 30-50% of the global CO_2 transfer velocity by assuming that the transfer velocity mediated by bubbles is proportional to the coverage rate of whitecaps. Reichel and Deike (2020) estimated that 40% of the CO_2 air–sea exchange fluxes in the Southern Ocean, North Atlantic and Pacific are mediated by bubbles. This discrepancy could be attributed to gas solubility, as the flux of less soluble gases is more enhanced by pressure effects (bubbles

Field Code Changed

Field Code Changed

are compressed by hydrostatic pressure) than more soluble gases (Bell et al., 2017; Reichel and Deike, 2020).

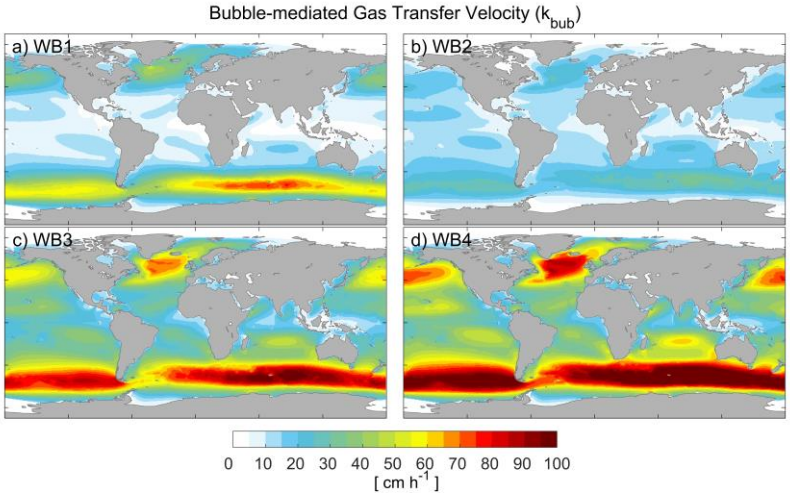

Figure 2. The annual mean bubble-mediated gas transfer velocity in unit of cm h^{-1}. The different bubble-mediated parameterizations include a) ~~DM18~~WB1; b) ~~W97~~WB2; c) ~~AW98~~WB3 and d) ~~A02~~WB4.

3.3 Wind speed dependence of k_{Hg^0} ~~k_{Hg}~~

Field Code Changed

Most of the studies parameterize transfer velocity with 10 meter wind speed through linear ($k_w = 2.8 \cdot u_{10} - 9.6$, for 3.6< u_{10} <13 m s^{-1}, Liss and Merlivat, 1986), quadratic ($k_w = 0.222 \cdot u_{10}^{\ 2} + 0.333 \cdot u_{10}$, Nightingale et al., 2000), or cubic relationships ($k_w = 0.026 \cdot u_{10}^{\ 3} + 3.3$, McGillis et al., 2001). Gaps among wind-based equations especially at developed wind-sea states cause high uncertainty in different models. Recent research has shown that the transfer velocities of Hg^0 ~~have a stronger dependence on~~are more sensitive to wind speed (with higher index) by using eddy covariance flux measurements ($k_w = 0.18 \cdot u_{10}^{\ 3}$, Osterwalder et al., 2021). Additional forcing factors, such as wave breaking and sea surface activators, may result in different transport characteristics for different gases. In this section, sea surface temperature (SST), TOC concentration and Hs of Case 1–4 are treated as random variables to fit the air–sea flux to the 10-meter wind speed using power functions (Fig. 3):

~~P18~~SUR1+~~DM18~~WB1: $k_w = 0.181 \cdot u_{10}^{\ 2.54}, r^2 = 0.893;$ ~~(15)~~(18)

~~P18~~SUR1+~~W97~~WB2: $k_w = 0.362 \cdot u_{10}^{\ 2.10}, r^2 = 0.963;$ ~~(16)~~(19)

~~P18~~SUR1+~~AW98~~WB3: $k_w = 0.426 \cdot u_{10}^{\ 2.33}, r^2 = 0.905;$ ~~(17)~~(20)

~~P18~~SUR1+~~A02~~WB4: $k_w = 0.487 \cdot u_{10}^{\ 2.34}, r^2 = 0.901$ ~~(18)~~(21)

Considering sea surface films and microscale wave breaking, the relationship between Hg^0 exchange velocity and wind speed appears to be between quadratic (Fig. 3a) and cubic (Fig. 3b and 3c), indicating a stronger dependence than suggested by the typically used parameterizations (Nightingale et al., 2000; McGillis et al., 2001). Compared with previous parameterizations (Fig. 3a and 3b), new parameterizations (Fig. 3d–g, Fig. S2) show higher transfer velocity especially at high wind speeds, but ~~it is~~ lower than that directly observed by Osterwalder et al. (2021; Fig. 3c) when wind speeds exceed 3–5 m/s. The new parameterization suggests that bubble effects play an important role in boosting Hg^0 air–sea exchange and become more important at high wind speeds. Some previous parameterization schemes may underestimate Hg^0 emissions when wind speeds are high enough to induce wave breaking. In comparison to gases with higher solubility such as CO_2, the air–sea exchange rate of Hg exhibits a stronger dependence on wind speed, consistent with the findings of Osterwalder et al. (2021). Indeed, microscale wave breaking enhances the transport velocity of poorly soluble gases, and bubble formation is more effective at high wind speeds.

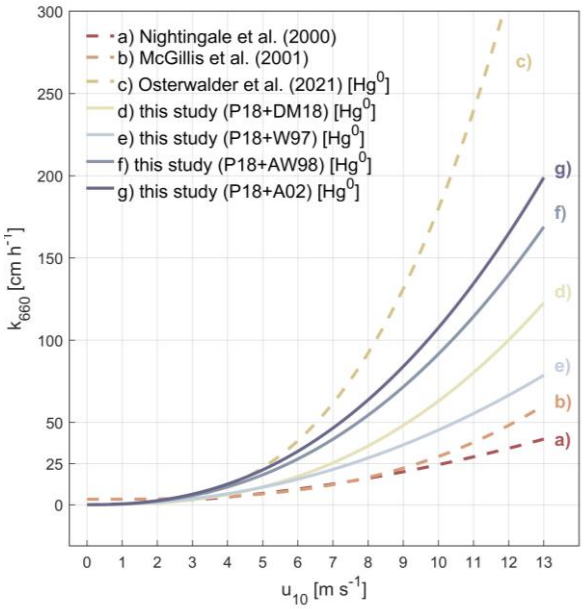

Figure 3. Wind speed dependence of transfer velocities used in gas exchange models to calculate air–sea fluxes. The k-values are normalized to Schmidt number of 660 (20 °C for CO_2 in seawater) and displayed against horizontal wind speed at 10 m [u_{10}]. For comparison, other wind speed relationships of the transfer velocity calculated by Nightingale et al. (2000), McGillis et al. (2001) and the cubic fit to measured transfer velocities of Hg^0 during two days of relaxed eddy accumulation Hg^0 emission measurements (Osterwalder et al., 2021) are included (dash line a-c). Solid curves d–g are the power fit to different model parametrization (Case 1–4). Case 1–4 have included the effect of wave breaking and surfactants. All four schemes employ the same surfactant parameterization ~~DM18~~WB1 and four different bubble parameterizations (~~DM18~~WB1, ~~W97~~WB2, ~~AW98~~WB3 and ~~A02~~WB4).

3.4 Hg^0 exchange flux difference

The baseline model generally captures the spatial patterns of Hg^0 exchange flux (Fig. 4a), with lower

flux in equator and polar regions and higher flux in mid-latitudes, which basically corresponds with the distribution of kw_{Hg^0} ~~kw~~. Fig. 4b–d illustrates the simulated Hg^0 exchange fluxes by Case ~~5~~A ~~7~~ C compared with the baseline. The inclusion of the sea surfactant suppression effect alone results in a reduced flux in most areas, with the largest reduction in the North Atlantic, reaching -9% (Fig. 4b). However, the impact on a global level is minor, with only a 0.9% reduction in the global net Hg air–sea exchange flux compared with the baseline (3841 Mg a^{-1}), which equals to 3808 Mg a^{-1}. When only considering the effect of wave breaking (Fig. 4c and 4d), the exchange fluxes are estimated to be 4070 Mg a^{-1} and 4189 Mg a^{-1}, respectively. Such values indicate an increase of 4.5% and 11.1% in global Hg exchange fluxes. The increased Hg^0 evasion may increase atmospheric Hg concentrations and thus Hg deposition ~~and lifetime~~, as well as prolong Hg lifetime in biogeochemical cycles. Since only the oceanic part is considered in this model, i.e. Hg^0 deposition and atmospheric Hg^0 concentration as external forcing does not change with time, the increase in air–sea exchange fluxes significantly reduce the concentration of Hg^0 in the surface ocean (0–100 m; t test on means, $p<0.001$; Fig. S3), and thus alter other ocean Hg reservoirs (Fig. S4) and budgets (Fig. S5). This will result in an augmentation of the magnitude of exchange flux changes, as effective bubble mediated transfer in the regions of most developed wind-sea state significantly increase Hg^0 transfer velocity (t test on means, $p<0.001$), while the impact of decreased concentration outweighs the slightly increased kw_{Hg^0} ~~kw~~ where the waves are not well developed. As the result, the local variations of Case ~~5~~ B and CascC~~6~~ range from -22.2% to 40.5% and -28.3% to 53.1%. We conclude that the model changes are primarily due to the inclusion of bubble effect, whereas the inclusion of sea surface surfactants has a comparatively negligible impact on the variations in air–sea exchange fluxes.

The global net fluxes based upon the combined effect of wave breaking and surfactants (Case 1–4) show similar spatial patterns with baseline but present higher values (Fig. S6 and Fig. S7). The fluxes are 4056 Mg a^{-1}, 4016 Mg a^{-1}, 4155 Mg a^{-1} and 4184 Mg a^{-1}, respectively, which are 5.6%, 4.6%, 8.2% and 8.9% higher than the baseline (3841 Mg a^{-1}) because of the higher kw_{Hg^0} ~~kw~~ (Fig. S8). These values are also higher than the estimates of 3360 Mg a^{-1} by Zhang et al. (2023) and 3950 Mg a^{-1} by Horowitz et al. (2017). The local variations range from -21.8 to 39.5%, -16.2% to 28%, -28% to 51.3% and -30.7% to 56.2%, respectively. However, all the modeled fluxes from Case 1 to Case 4 and baseline are within the large uncertainty range of the observations, so we cannot determine which parameterization scheme provides a more accurate estimate of air–sea exchange velocity simply by considering the current simulated results in conjunction with the available flux observations. Indeed, the fluxes are highly sensitive to concentration gradients and prevailing environmental conditions (wind speed, wave height and surfactant concentration) with high-frequency temporal variability, modelling therefore could represent rather general zonal distribution (Fig. 4a and Fig. S6) than precise figures due to spatial and temporal resolution limitations. For instance, during summer in the Southern Ocean, the seawater can even be under-saturated, leading to a net deposition of Hg from the atmosphere (Mastromonaco et al., 2017). This is not accurately reflected in the annual mean flux modeled in our study. However, our study might explain why different researches display great uncertainty in estimating Hg^0 exchange flux, as they

Field Code Changed

Field Code Changed

Field Code Changed

ignored the effect of surfactants and wave breaking. Therefore, further direct field measurements (especially micro-meteorology techniques) are necessary to assess the transfer velocity of Hg^0, as well as the simultaneous observation of surfactants and sea waves.

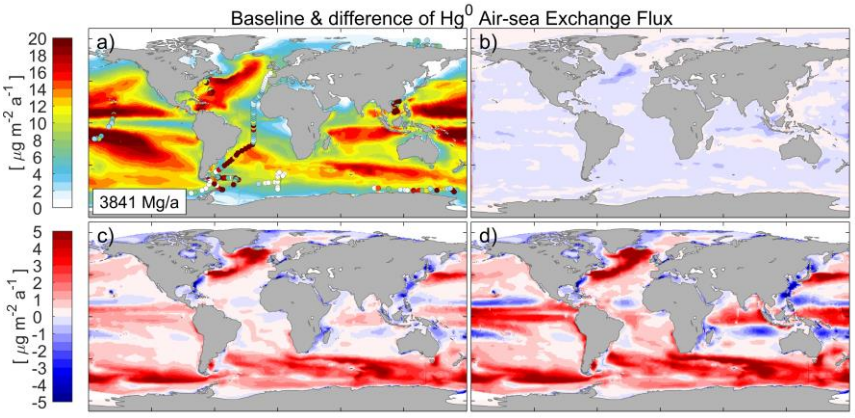

Figure 4. a) comparison between baseline model and observations (filled circles) for net Hg^0 air–sea exchange. Panels (b–d) are difference of annual mean net Hg^0 evasion flux with Baseline Model simulated by Case ~~5~~A ~~7~~ C which b) solely consider the effect of surfactant (~~Case5~~CaseA) with ~~P18~~ SUR1 parameterization and c) wave breaking with ~~DM18~~WB1 (Case ~~6~~B) and ~~AW98~~WB3 (Case ~~7~~C) parameterizations.

3.5 Model Uncertainty

Nightingale's parameterization was developed from in situ experiments utilizing both volatile and nonvolatile tracers, which potentially incorporate effects from wave breaking. However, they assumed that the transfer velocity only depends on diffusivity without taking solubility effect into consideration. This assumption may not be valid in the presence of breaking waves. Although our scheme may result in a potential overestimation of the wave-related contributions at lower wind speeds, it has the advantage of distinguishing between different relationships with wind speed—such as linear or quadratic dependencies for non-wave processes and cubic dependencies for wave breaking—particularly at high wind speeds.

T~~T~~he parameterization of the surfactant suppression is quite challenging, because significant spatial-temporal variations in surfactants and changes in the chemical composition of surfactants may affect the relationship between TOC concentration and surfactant concentration (Barthelmess et al., 2022), as well as the inhibition relationship of the sea surface film (Mustaffa et al., 2019). Since the composition of surfactant in the Atlantic Ocean may differ from other regions, extrapolating experimental findings on biological surfactants from the Atlantic Ocean to a global scale may introduce uncertainty. There is a risk of underestimating the suppressive effects of surfactants in coastal regions, as shown by Mustaffa et al. (2019), who found that the suppression of kw was in coastal waters compared to oceanic waters. Barthelmess et al. (2022) also ~~implied~~ showed that refractory DOC from coastal land sources has a more persistent impact on air–sea exchange, while the inhibitory effect of semi-unstable organic matter

(dissolved glucose and isoleucine) produced by phytoplankton is stronger but has a shorter impact time. ~~The highly spatial-temporal variations in short-term and seasonal of surfactants and the chemical composition of the surfactant pool further increase uncertainty.~~ On the other hand, wave breaking and bubble effect also show significant regional differences in the open sea and coastal waters (Callaghan et al., 2008; Woolf, 2005). The high-frequency temporal variability of the wind-wave processes and the limited resolution of wind-wave data used in this study may underestimate the variability caused by weather-scale Hg^0 transport. Currently, there is still a lack of quantitative research on the effects of different surfactant components and bubble effects on air–sea exchange. More detailed measurements of air–sea exchange velocity and related physical quantities are needed to better understand the importance of bubble-mediated and sea surface film-mediated Hg exchange. In addition, since only the ocean part is considered, the atmospheric Hg^0 concentration and deposition remain constant over time, which affect flux calculations to a substantially higher degree (Soerensen et al., 2013). To address this limitation, employing a coupled online model (Zhang et al., 2019), proves to be a valuable strategy for achieving a more accurate simulation of Hg^0 flux.

4 Conclusion

The estimation of Hg^0 air–sea exchange is of great uncertainty since wind speed is currently the only used~~The estimation of Hg^0 air–sea exchange is of great uncertainty since only wind speed is the only parameter~~. Sea surfactants and breaking waves are thought to be two of the biggest drivers of uncertainty. In order to better assess the influence of surfactants and waves on Hg^0 air–sea exchange, we integrate sea surfactants and wave breaking processes into the air-sea exchange process of Hg^0 within the MIT General Circulation Model (MITgcm). Seven experiments (four combined experiments and three ~~sensitive~~ sensitivity experiments) were conducted to explore the influence of sea surfactants and wave breaking on Hg^0 air–sea exchange flux.

We find that surfactants can reduce the transfer velocity of Hg^0 by 0–16.7%. However, wave breaking has a much more significant impact, increasing the transfer velocity by 1–3 times due to the low solubility of Hg.~~We find that the Hg^0 transfer velocity can be suppressed by surfactants for 0–16.7%, while wave breaking contribute a much greater influence on it, as it is significantly increased 1–3 times because of low solubility of Hg.~~ Therefore, we note that lack of consideration of these processes may lead to a vast underestimation of Hg^0 air-sea exchange flux. The new simulations that include sea surfactants and wave breaking show a much higher transfer velocity of Hg^0 and a higher dependence of Hg on wind, consistent with latest observations. Hg^0 air–sea exchange flux is increased in mid- to high-latitude regions with high wind and wave breaking efficiency (28–56~~%),~~ %). Conversely, in low-latitude regions with lower wind speeds and in nearshore areas with reduced wave activity, the flux decreases by 16–31% as the surface concentration of Hg^0 diminishes due to higher emissions~~while it is reduced by concentration change at low latitudes with low wind speeds and nearshore areas with low wave heights (16–31%)~~. The global mean Hg^0 fluxes are 4016–4184 Mg a^{-1}, respectively, which are 4.6–8.9% higher than the baseline (3841

Formatted: Superscript

Formatted: Superscript

Mg a^{-1}). It should be pointed out that our study doesn't consider changes in atmospheric Hg, and the decreases in marine Hg concentrations offset the change in transfer velocities. Therefore, we believe that the global mean Hg^0 air-sea exchange flux will be even higher.

The results explain why different researches give such different schemes of kw_{Hg^0} kw. The omission of the influences of waves and surfactants during the experiment may resulted in a significant discrepancy when using wind speed as the only parameter in the estimation of gas exchange velocity.when using wind speed as the exclusive proxy. Theoretically, our study explains the variation among different researches and provides a universal scheme for predicting air–sea exchange transfer velocity. In addition, our parameterization schemes highlight significant uncertainty in the parameterization of surfactants and wave breaking. Traditional indirect methods, such as bulk or enclosure (flux chambers) approaches, and commonly employed flux parameterization, are insufficient for effectively constraining Hg^0 air–sea exchange flux. Thus, we highlight the necessity for direct high-resolution measurements of Hg^0 flux, especially synchronous observation of other parameter like wave height, surfactant concentration and chemical composition. Because of the high sensitivity to different parameterizations at middle and high latitudes, especially in the North Atlantic (Fig. 4), we believe that synchronous observations in these regions may be helpful for modelers to develop and validate robust models for simulating the diel, seasonal and inter-annual Hg dynamics on a local to regional scale.Thus, we highlight the necessity for direct high-resolution measurements of Hg^0 flux, especially simultaneous observation of other parameter like wave height, surfactant concentration and chemical composition, as they are essential for modelers to develop and validate robust models for simulating the diel, seasonal and inter-annual Hg dynamics on a local to regional scale.

Field Code Changed

Formatted: Superscript

Code and data availability

The MITgcm model code is available at https://github.com/MITgcm/MITgcm.git (last access: 16 May 2024). Other code and datasets in this paper is permanently archived on Zenodo at https://doi.org/10.5281/zenodo.11046795 (Li and Zhang, 2024). The data supporting the findings of this study are available within the article and its Supplement.

Author contribution

YZ and LL conceived the project, and YZ supervised and administered the project. YZ and LL modified the code. LL performed the simulations with help by PW and PZ. YZ and LL conducted the analysis, and wrote the paper. YZ and SH helped with discussions and with revising the paper.

Competing interests. The author has declared that there are no competing interests.

Acknowledgments

This study is supported by the National Natural Science Foundation of China (42177349), the Fundamental Research Funds for the Central Universities (Grant nos. 14380188 and 14380168), the Frontiers Science Center for Critical Earth Material Cycling, and the Collaborative Innovation Center of Climate Change, Jiangsu Province.

References

Amos, H. M., Jacob, D. J., Streets, D. G., and Sunderland, E. M.: Legacy impacts of all-time anthropogenic emissions on the global mercury cycle: GLOBAL IMPACTS OF LEGACY MERCURY, Global Biogeochem. Cycles, 27, 410–421, https://doi.org/10.1002/gbc.20040, 2013.

Amos, H. M., Sonke, J. E., Obrist, D., Robins, N., Hagan, N., Horowitz, H. M., Mason, R. P., Witt, M., Hedgecock, I. M., Corbitt, E. S., and Sunderland, E. M.: Observational and Modeling Constraints on Global Anthropogenic Enrichment of Mercury, Environ. Sci. Technol., 49, 4036–4047, https://doi.org/10.1021/es5058665, 2015.

Andersson, M. E., Gårdfeldt, K., Wängberg, I., and Strömberg, D.: Determination of Henry's law constant for elemental mercury, Chemosphere, 73, 587–592, https://doi.org/10.1016/j.chemosphere.2008.05.067, 2008.

Asher, W., Edson, J., Mcgillis, W., Wanninkhof, R., Ho, D. T., and Litchendor, T.: Fractional Area Whitecap Coverage and Air-Sea Gas Transfer Velocities Measured During GasEx-98, in: Geophysical Monograph Series, edited by: Donelan, M. A., Drennan, W. M., Saltzman, E. S., and Wanninkhof, R., American Geophysical Union, Washington, D. C., 199–203, https://doi.org/10.1029/GM127p0199, ~~2013~~2002.

Asher, W. E. and Wanninkhof, R.: The effect of bubble-mediated gas transfer on purposeful dual-gaseous tracer experiments, J. Geophys. Res., 103, 10555–10560, https://doi.org/10.1029/98JC00245, 1998.

Asher, W. E., Karle, L. M., Higgins, B. J., Farley, P. J., Monahan, E. C., and Leifer, I. S.: The influence of bubble plumes on air-seawater gas transfer velocities, J. Geophys. Res., 101, 12027–12041, https://doi.org/10.1029/96JC00121, 1996.

Barthelmeß, T. and Engel, A.: How biogenic polymers control surfactant dynamics in the surface microlayer: insights from a coastal Baltic Sea study, Biogeosciences, 19, 4965–4992, https://doi.org/10.5194/bg-19-4965-2022, 2022.

Barthelmeß, T., Schütte, F., and Engel, A.: Variability of the Sea Surface Microlayer Across a Filament's Edge and Potential Influences on Gas Exchange, Front. Mar. Sci., 8, 718384, https://doi.org/10.3389/fmars.2021.718384, 2021.

Battino, R.: The Ostwald coefficient of gas solubility, Fluid Phase Equilibria, 15, 231–240, https://doi.org/10.1016/0378-3812(84)87009-0, 1984.

Bell, T. G., Landwehr, S., Miller, S. D., De Bruyn, W. J., Callaghan, A. H., Scanlon, B., Ward, B., Yang, M., and Saltzman, E. S.: Estimation of bubble-mediated air–sea gas exchange from concurrent DMS and CO₂ transfer velocities at intermediate–high wind speeds, Atmos. Chem. Phys., 17, 9019–9033, https://doi.org/10.5194/acp-17-9019-2017, 2017.

Blomquist, B. W., Brumer, S. E., Fairall, C. W., Huebert, B. J., Zappa, C. J., Brooks, I. M., Yang, M., Bariteau, L., Prytherch, J., Hare, J. E., Czerski, H., Matei, A., and Pascal, R. W.: Wind Speed and Sea State Dependencies of Air-Sea Gas Transfer: Results From the High Wind Speed Gas Exchange Study

(HiWinGS), JGR Oceans, 122, 8034–8062, https://doi.org/10.1002/2017JC013181, 2017.

Brumer, S. E., Zappa, C. J., Blomquist, B. W., Fairall, C. W., Cifuentes-Lorenzen, A., Edson, J. B., Brooks, I. M., and Huebert, B. J.: Wave-Related Reynolds Number Parameterizations of CO 2 and DMS Transfer Velocities, Geophys. Res. Lett., 44, 9865–9875, https://doi.org/10.1002/2017GL074979, 2017.

Callaghan, A., De Leeuw, G., Cohen, L., and O'Dowd, C. D.: Relationship of oceanic whitecap coverage to wind speed and wind history, Geophys. Res. Lett., 35, L23609, https://doi.org/10.1029/2008GL036165, 2008.

Calleja, M. L., Duarte, C. M., Prairie, Y. T., Agustı, S., and Herndl, G. J.: Evidence for surface organic matter modulation of air-sea CO2 gas exchange, 2009.

Deike, L. and Melville, W. K.: Gas Transfer by Breaking Waves, Geophysical Research Letters, 45, https://doi.org/10.1029/2018GL078758, 2018.

Dittmar, T. and Kattner, G.: The biogeochemistry of the river and shelf ecosystem of the Arctic Ocean: a review, Marine Chemistry, 83, 103–120, https://doi.org/10.1016/S0304-4203(03)00105-1, 2003.

Dutkiewicz, S., Ward, B. A., Monteiro, F., and Follows, M. J.: Interconnection of nitrogen fixers and iron in the Pacific Ocean: Theory and numerical simulations: MARINE NITROGEN FIXERS AND IRON, Global Biogeochem. Cycles, 26, n/a-n/a, https://doi.org/10.1029/2011GB004039, 2012.

Edson, J. B., Fairall, C. W., Bariteau, L., Zappa, C. J., Cifuentes-Lorenzen, A., McGillis, W. R., Pezoa, S., Hare, J. E., and Helmig, D.: Direct covariance measurement of CO 2 gas transfer velocity during the 2008 Southern Ocean Gas Exchange Experiment: Wind speed dependency, J. Geophys. Res., 116, C00F10, https://doi.org/10.1029/2011JC007022, 2011.

Edson, J. B., Jampana, V., Weller, R. A., Bigorre, S. P., Plueddemann, A. J., Fairall, C. W., Miller, S. D., Mahrt, L., Vickers, D., and Hersbach, H.: On the Exchange of Momentum over the Open Ocean, Journal of Physical Oceanography, 43, 1589–1610, https://doi.org/10.1175/JPO-D-12-0173.1, 2013.

Engel, A., Bange, H. W., Cunliffe, M., Burrows, S. M., Friedrichs, G., Galgani, L., Herrmann, H., Hertkorn, N., Johnson, M., Liss, P. S., Quinn, P. K., Schartau, M., Soloviev, A., Stolle, C., Upstill-Goddard, R. C., Van Pinxteren, M., and Zäncker, B.: The Ocean's Vital Skin: Toward an Integrated Understanding of the Sea Surface Microlayer, Front. Mar. Sci., 4, 165, https://doi.org/10.3389/fmars.2017.00165, 2017.

Forget, G., Campin, J.-M., Heimbach, P., Hill, C. N., Ponte, R. M., and Wunsch, C.: ECCO version 4: an integrated framework for non-linear inverse modeling and global ocean state estimation, Geosci. Model Dev., 8, 3071–3104, https://doi.org/10.5194/gmd-8-3071-2015, 2015.

Frew, N. M.: The role of organic films in air–sea gas exchange, in: The Sea Surface and Global Change, edited by: Liss, P. S. and Duce, R. A., Cambridge University Press, 121–172, https://doi.org/10.1017/CBO9780511525025.006, 1997.

Gašparović, B., Kozarac, Z., Saliot, A., Ćosović, B., and Möbius, D.: Physicochemical Characterization of Natural andex-SituReconstructed Sea-Surface Microlayers, Journal of Colloid and Interface Science,

208, 191–202, https://doi.org/10.1006/jcis.1998.5792, 1998.

Hansell, D., Carlson, C., Repeta, D., and Schlitzer, R.: Dissolved Organic Matter in the Ocean: A Controversy Stimulates New Insights, Oceanog., 22, 202–211, https://doi.org/10.5670/oceanog.2009.109, 2009.

Hersbach, H., Bell, B., Berrisford, P., Hirahara, S., Horányi, A., Muñoz-Sabater, J., Nicolas, J., Peubey, C., Radu, R., Schepers, D., Simmons, A., Soci, C., Abdalla, S., Abellan, X., Balsamo, G., Bechtold, P., Biavati, G., Bidlot, J., Bonavita, M., De Chiara, G., Dahlgren, P., Dee, D., Diamantakis, M., Dragani, R., Flemming, J., Forbes, R., Fuentes, M., Geer, A., Haimberger, L., Healy, S., Hogan, R. J., Hólm, E., Janisková, M., Keeley, S., Laloyaux, P., Lopez, P., Lupu, C., Radnoti, G., De Rosnay, P., Rozum, I., Vamborg, F., Villaume, S., and Thépaut, J.: The ERA5 global reanalysis, Quart J Royal Meteoro Soc, 146, 1999–2049, https://doi.org/10.1002/qj.3803, 2020.

Horowitz, H. M., Jacob, D. J., Zhang, Y., Dibble, T. S., Slemr, F., Amos, H. M., Schmidt, J. A., Corbitt, E. S., Marais, E. A., and Sunderland, E. M.: A new mechanism for atmospheric mercury redox chemistry: implications for the global mercury budget, Atmos. Chem. Phys., 17, 6353–6371, https://doi.org/10.5194/acp-17-6353-2017, 2017.

Jahne, B., Münnich, K. O., and Siegenthaler, U.: Measurements of gas exchange and momentum transfer in a circular wind-water tunnel, Tellus, 31, 321–329, https://doi.org/10.1111/j.2153-3490.1979.tb00911.x, 1979.

Jeffery, C. D., Robinson, I. S., and Woolf, D. K.: Tuning a physically-based model of the air–sea gas transfer velocity, Ocean Modelling, 31, 28–35, https://doi.org/10.1016/j.ocemod.2009.09.001, 2010.

Kalinchuk, V. V., Lopatnikov, E. A., Astakhov, A. S., Ivanov, M. V., and Hu, L.: Distribution of atmospheric gaseous elemental mercury (Hg(0)) from the Sea of Japan to the Arctic, and Hg(0) evasion fluxes in the Eastern Arctic Seas: Results from a joint Russian-Chinese cruise in fall 2018, Science of The Total Environment, 753, 142003, https://doi.org/10.1016/j.scitotenv.2020.142003, 2021.

Kihm, C. and Körtzinger, A.: Air-sea gas transfer velocity for oxygen derived from float data, J. Geophys. Res., 115, 2009JC006077, https://doi.org/10.1029/2009JC006077, 2010.

Kock, A., Schafstall, J., Dengler, M., Brandt, P., and Bange, H. W.: Sea-to-air and diapycnal nitrous oxide fluxes in the eastern tropical North Atlantic Ocean, Biogeosciences, 9, 957–964, https://doi.org/10.5194/bg-9-957-2012, 2012.

Krall, K. E. and Jähne, B.: First laboratory study of air–sea gas exchange at hurricane wind speeds, Ocean Sci., 10, 257–265, https://doi.org/10.5194/os-10-257-2014, 2014.

Kurata, N., Vella, K., Hamilton, B., Shivji, M., Soloviev, A., Matt, S., Tartar, A., and Perrie, W.: Surfactant-associated bacteria in the near-surface layer of the ocean, Sci Rep, 6, https://doi.org/10.1038/srep19123, 2016.

Kuss, J., Zülicke, C., Pohl, C., and Schneider, B.: Atlantic mercury emission determined from continuous analysis of the elemental mercury sea-air concentration difference within transects between 50°N and

50°S: ATLANTIC Hg SEA-AIR CONCENTRATION DIFFERENCE, Global Biogeochem. Cycles, 25, n/a-n/a, https://doi.org/10.1029/2010GB003998, 2011.

Lavoie, R. A., Jardine, T. D., Chumchal, M. M., Kidd, K. A., and Campbell, L. M.: Biomagnification of Mercury in Aquatic Food Webs: A Worldwide Meta-Analysis, Environ. Sci. Technol., 47, 13385–13394, https://doi.org/10.1021/es403103t, 2013.

Li, S., Babanin, A. V., Qiao, F., Dai, D., Jiang, S., and Guan, C.: Laboratory experiments on CO2 gas exchange with wave breaking, Journal of Physical Oceanography, https://doi.org/10.1175/JPO-D-20-0272.1, 2021.

Lin, I.-I., Wen, L.-S., Liu, K.-K., Tsai, W.-T., and Liu, A. K.: Evidence and quantification of the correlation between radar backscatter and ocean colour supported by simultaneously acquired in situ sea truth: CORRELATION BETWEEN RADAR BACKSCATTER AND OCEAN COLOUR, Geophys. Res. Lett., 29, 102-1-102–4, https://doi.org/10.1029/2001GL014039, 2002.

Liss, P. S. and Merlivat, L.: Air-Sea Gas Exchange Rates: Introduction and Synthesis, in: The Role of Air-Sea Exchange in Geochemical Cycling, edited by: Buat-Ménard, P., Springer Netherlands, Dordrecht, 113–127, https://doi.org/10.1007/978-94-009-4738-2_5, 1986.

Loose, B., McGillis, W. R., Perovich, D., Zappa, C. J., and Schlosser, P.: A parameter model of gas exchange for the seasonal sea ice zone, Ocean Sci., 10, 17–28, https://doi.org/10.5194/os-10-17-2014, 2014.

McGillis, W. R., Edson, J. B., Ware, J. D., Dacey, J. W. H., Hare, J. E., Fairall, C. W., and Wanninkhof, R.: Carbon dioxide flux techniques performed during GasEx-98, Marine Chemistry, 75, 267–280, https://doi.org/10.1016/S0304-4203(01)00042-1, 2001.

McKenna, S. P. and McGillis, W. R.: The role of free-surface turbulence and surfactants in air–water gas transfer, International Journal of Heat and Mass Transfer, 47, 539–553, https://doi.org/10.1016/j.ijheatmasstransfer.2003.06.001, 2004.

Mesarchaki, E., Kräuter, C., Krall, K. E., Bopp, M., Helleis, F., Williams, J., and Jähne, B.: Measuring air–sea gas-exchange velocities in a large-scale annular wind–wave tank, Ocean Sci., 11, 121–138, https://doi.org/10.5194/os-11-121-2015, 2015.

Monahan, E. C., and D. K. Woolf: Comments on "Variations of Whitecap Coverage with Wind stress and Water Temperature. J. Phys. Oceanogr., 19, 706–709, https://doi.org/10.1175/1520-0485(1989)019<0706:COOWCW>2.0.CO;2, 1989.

Mustaffa, N. I. H., Ribas-Ribas, M., Banko-Kubis, H. M., and Wurl, O.: Global reduction of in situ CO 2 transfer velocity by natural surfactants in the sea-surface microlayer, Proc. R. Soc. A., 476, 20190763, https://doi.org/10.1098/rspa.2019.0763, 2020.

Nerentorp Mastromonaco, M. G., Gårdfeldt, K., and Langer, S.: Mercury flux over West Antarctic Seas during winter, spring and summer, Marine Chemistry, 193, 44–54, https://doi.org/10.1016/j.marchem.2016.08.005, 2017.

Nightingale, P. D., Malin, G., Law, C. S., Watson, A. J., Liss, P. S., Liddicoat, M. I., Boutin, J., and Upstill-Goddard, R. C.: In situ evaluation of air-sea gas exchange parameterizations using novel conservative and volatile tracers, Global Biogeochem. Cycles, 14, 373–387, https://doi.org/10.1029/1999GB900091, 2000.

Osterwalder, S., Nerentorp, M., Zhu, W., Jiskra, M., Nilsson, E., Nilsson, M. B., Rutgersson, A., Soerensen, A. L., Sommar, J., Wallin, M. B., Wängberg, I., and Bishop, K.: Critical Observations of Gaseous Elemental Mercury Air-Sea Exchange, Global Biogeochemical Cycles, 35, https://doi.org/10.1029/2020GB006742, 2021.

Pereira, R., Schneider-Zapp, K., and Upstill-Goddard, R. C.: Surfactant control of gas transfer velocity along an offshore coastaltransect: results from a laboratory gas exchange tank, Biogeosciences, 13, 3981–3989, https://doi.org/10.5194/bg-13-3981-2016, 2016.

Pereira, R., Ashton, I., Sabbaghzadeh, B., Shutler, J. D., and Upstill-Goddard, R. C.: Reduced air–sea CO2 exchange in the Atlantic Ocean due to biological surfactants, Nature Geosci, 11, 492–496, https://doi.org/10.1038/s41561-018-0136-2, 2018.

Poissant, L., Amyot, M., Pilote, M., and Lean, D.: Mercury Water−Air Exchange over the Upper St. Lawrence River and Lake Ontario, Environ. Sci. Technol., 34, 3069–3078, https://doi.org/10.1021/es990719a, 2000.

Reichl, B. G. and Deike, L.: Contribution of Sea-State Dependent Bubbles to Air-Sea Carbon Dioxide Fluxes, Geophys. Res. Lett., 47, https://doi.org/10.1029/2020GL087267, 2020.

Sabbaghzadeh, B., Upstill-Goddard, R. C., Beale, R., Pereira, R., and Nightingale, P. D.: The Atlantic Ocean surface microlayer from 50°N to 50°S is ubiquitously enriched in surfactants at wind speeds up to 13 m s −1: Atlantic Ocean Surfactants, Geophys. Res. Lett., 44, 2852–2858, https://doi.org/10.1002/2017GL072988, 2017.

Salter, M. E., Upstill-Goddard, R. C., Nightingale, P. D., Archer, S. D., Blomquist, B., Ho, D. T., Huebert, B., Schlosser, P., and Yang, M.: Impact of an artificial surfactant release on air-sea gas fluxes during Deep Ocean Gas Exchange Experiment II, J. Geophys. Res., 116, 2011JC007023, https://doi.org/10.1029/2011JC007023, 2011.

Satpute, S. K., Banat, I. M., Dhakephalkar, P. K., Banpurkar, A. G., and Chopade, B. A.: Biosurfactants, bioemulsifiers and exopolysaccharides from marine microorganisms, Biotechnology Advances, 2010.

Schmidt, R. and Schneider, B.: The effect of surface films on the air–sea gas exchange in the Baltic Sea, Marine Chemistry, 126, 56–62, https://doi.org/10.1016/j.marchem.2011.03.007, 2011.

Soerensen, A. L., Mason, R. P., Balcom, P. H., and Sunderland, E. M.: Drivers of Surface Ocean Mercury Concentrations and Air–Sea Exchange in the West Atlantic Ocean, Environ. Sci. Technol., 47, 7757–7765, https://doi.org/10.1021/es401354q, 2013.

Soerensen, A. L., Mason, R. P., Balcom, P. H., Jacob, D. J., Zhang, Y., Kuss, J., and Sunderland, E. M.: Elemental Mercury Concentrations and Fluxes in the Tropical Atmosphere and Ocean, Environ. Sci.

Technol., 48, 11312–11319, https://doi.org/10.1021/es503109p, 2014.

Tsai, W.: An assessment of the effect of sea surface surfactant on global atmosphere-ocean CO 2 flux, J. Geophys. Res., 108, 3127, https://doi.org/10.1029/2000JC000740, 2003.

Vagle, S., McNeil, C., and Steiner, N.: Upper ocean bubble measurements from the NE Pacific and estimates of their role in air-sea gas transfer of the weakly soluble gases nitrogen and oxygen, J. Geophys. Res., 115, 2009JC005990, https://doi.org/10.1029/2009JC005990, 2010.

Wang, C., Wang, Z., Hui, F., and Zhang, X.: Speciated atmospheric mercury and sea–air exchange of gaseous mercury in the South China Sea, Atmos. Chem. Phys., 19, 10111–10127, https://doi.org/10.5194/acp-19-10111-2019, 2019.

Wang, J., Xie, Z., Wang, F., and Kang, H.: Gaseous elemental mercury in the marine boundary layer and air-sea flux in the Southern Ocean in austral summer, Science of The Total Environment, 603–604, 510–518, https://doi.org/10.1016/j.scitotenv.2017.06.120, 2017.

Wanninkhof, R.: Relationship between wind speed and gas exchange over the ocean, J. Geophys. Res., 97, 7373, https://doi.org/10.1029/92JC00188, 1992.

Wanninkhof, R., Asher, W. E., Ho, D. T., Sweeney, C., and McGillis, W. R.: Advances in Quantifying Air-Sea Gas Exchange and Environmental Forcing, Annu. Rev. Mar. Sci., 1, 213–244, https://doi.org/10.1146/annurev.marine.010908.163742, 2009.

Wilke, C. R. and Chang, P.: Correlation of diffusion coefficients in dilute solutions, AIChE J., 1, 264–270, https://doi.org/10.1002/aic.690010222, 1955.

Woolf, D. K.: Bubbles and their role in gas exchange, in: The Sea Surface and Global Change, edited by: Liss, P. S. and Duce, R. A., Cambridge University Press, 173–206, https://doi.org/10.1017/CBO9780511525025.007, 1997.

Woolf, D. K.: Parametrization of gas transfer velocities and sea-state-dependent wave breaking, Tellus B: Chemical and Physical Meteorology, 57, 87, https://doi.org/10.3402/tellusb.v57i2.16783, 2005.

Woolf, D. K. and Thorpe, S. A.: Bubbles and the air-sea exchange of gases in near-saturation conditions, J Mar Res, 49, 435–466, https://doi.org/10.1357/002224091784995765, 1991.

Woolf, D. K., Leifer, I. S., Nightingale, P. D., Rhee, T. S., Bowyer, P., Caulliez, G., De Leeuw, G., Larsen, S. E., Liddicoat, M., Baker, J., and Andreae, M. O.: Modelling of bubble-mediated gas transfer: Fundamental principles and a laboratory test, Journal of Marine Systems, 66, 71–91, https://doi.org/10.1016/j.jmarsys.2006.02.011, 2007.

Wurl, O., Wurl, E., Miller, L., Johnson, K., and Vagle, S.: Formation and global distribution of sea-surface microlayers, Biogeosciences, 8, 121–135, https://doi.org/10.5194/bg-8-121-2011, 2011.

Wurl, O., Stolle, C., Van Thuoc, C., The Thu, P., and Mari, X.: Biofilm-like properties of the sea surface and predicted effects on air–sea CO2 exchange, Progress in Oceanography, 144, 15–24, https://doi.org/10.1016/j.pocean.2016.03.002, 2016.

Wurl, O. and Obbard, J. P.: Chlorinated pesticides and PCBs in the sea-surface microlayer and seawater samples of Singapore, Marine Pollution Bulletin, 50, 1233–1243, https://doi.org/10.1016/j.marpolbul.2005.04.022, 2005.

Wurl, O., Ekau, W., Landing, W. M., and Zappa, C. J.: Sea surface microlayer in a changing ocean – A perspective, Elementa: Science of the Anthropocene, 5, 31, https://doi.org/10.1525/elementa.228, 2017.

Yang, M., Smyth, T. J., Kitidis, V., Brown, I. J., Wohl, C., Yelland, M. J., and Bell, T. G.: Natural variability in air–sea gas transfer efficiency of CO2, Sci Rep, 11, 13584, https://doi.org/10.1038/s41598-021-92947-w, 2021.

Zhang, W., Perrie, W., and Vagle, S.: Impacts of winter storms on air-sea gas exchange, Geophys. Res. Lett., 33, L14803, https://doi.org/10.1029/2005GL025257, 2006.

Zhang, Y., Jaeglé, L., and Thompson, L.: Natural biogeochemical cycle of mercury in a global three-dimensional ocean tracer model, Global Biogeochemical Cycles, 28, 553–570, https://doi.org/10.1002/2014GB004814, 2014.

Zhang, Y., Horowitz, H., Wang, J., Xie, Z., Kuss, J., and Soerensen, A. L.: A Coupled Global Atmosphere-Ocean Model for Air-Sea Exchange of Mercury: Insights into Wet Deposition and Atmospheric Redox Chemistry, Environ. Sci. Technol., 53, 5052–5061, https://doi.org/10.1021/acs.est.8b06205, 2019.

Zhang, Y., Soerensen, A. L., Schartup, A. T., and Sunderland, E. M.: A Global Model for Methylmercury Formation and Uptake at the Base of Marine Food Webs, Global Biogeochem. Cycles, 34, https://doi.org/10.1029/2019GB006348, 2020.

Zhang, Y., Zhang, P., Song, Z., Huang, S., Yuan, T., Wu, P., Shah, V., Liu, M., Chen, L., Wang, X., Zhou, J., and Agnan, Y.: An updated global mercury budget from a coupled atmosphere-land-ocean model: 40% more re-emissions buffer the effect of primary emission reductions, One Earth, 6, 316–325, https://doi.org/10.1016/j.oneear.2023.02.004, 2023.